AFRL-RI-RS-TR-2014-106

ROAD NETWORK CONFLATION BASED ON RADAR TRACKS

SYRACUSE UNIVERSITY

APRIL 2014

FINAL TECHNICAL REPORT

APPROVED FOR PUBLIC RELEASE; DISTRIBUTION UNLIMITED

STINFO COPY

AIR FORCE RESEARCH LABORATORY
INFORMATION DIRECTORATE

■ **AIR FORCE MATERIEL COMMAND** ■ **UNITED STATES AIR FORCE** ■ **ROME, NY 13441**

NOTICE AND SIGNATURE PAGE

Using Government drawings, specifications, or other data included in this document for any purpose other than Government procurement does not in any way obligate the U.S. Government. The fact that the Government formulated or supplied the drawings, specifications, or other data does not license the holder or any other person or corporation; or convey any rights or permission to manufacture, use, or sell any patented invention that may relate to them.

This report was cleared for public release by the 88th ABW, Wright-Patterson AFB Public Affairs Office and is available to the general public, including foreign nationals. Copies may be obtained from the Defense Technical Information Center (DTIC) (http://www.dtic.mil).

AFRL-RI-RS-TR-2014-106 HAS BEEN REVIEWED AND IS APPROVED FOR PUBLICATION IN ACCORDANCE WITH ASSIGNED DISTRIBUTION STATEMENT.

FOR THE DIRECTOR:

/ S /
ADNAN BUBALO
Work Unit Manager

/ S /
MICHAEL J. WESSING
Deputy Chief, Information Intelligence
Systems and Analysis Division
Information Directorate

This report is published in the interest of scientific and technical information exchange, and its publication does not constitute the Government's approval or disapproval of its ideas or findings.

REPORT DOCUMENTATION PAGE

Form Approved
OMB No. 0704-0188

1. REPORT DATE *(DD-MM-YYYY)*	2. REPORT TYPE	3. DATES COVERED *(From - To)*
APRIL 2014	FINAL TECHNICAL REPORT	DEC 2010 – DEC 2013

4. TITLE AND SUBTITLE

ROAD NETWORK CONFLATION BASED ON RADAR TRACKS

5a. CONTRACT NUMBER
FA8750-11-2-0081

5b. GRANT NUMBER
N/A

5c. PROGRAM ELEMENT NUMBER
62788F

6. AUTHOR(S)

Ruixin Niu and Pramod K. Varshney

5d. PROJECT NUMBER
E2DT

5e. TASK NUMBER
SU

5f. WORK UNIT NUMBER
RE

7. PERFORMING ORGANIZATION NAME(S) AND ADDRESS(ES)
Syracuse University, Office of Sponsored Programs
113 Bowne Hall, Syracuse University
Syracuse, NY 13244-1200

8. PERFORMING ORGANIZATION REPORT NUMBER

9. SPONSORING/MONITORING AGENCY NAME(S) AND ADDRESS(ES)

Air Force Research Laboratory/RIEA
525 Brooks Road
Rome NY 13441-4505

10. SPONSOR/MONITOR'S ACRONYM(S)
AFRL/RI

11. SPONSOR/MONITOR'S REPORT NUMBER
AFRL-RI-RS-TR-2014-106

12. DISTRIBUTION AVAILABILITY STATEMENT

Approved for Public Release; Distribution Unlimited. PA# 88ABW-2014-1856
Date Cleared: 22 APR 2014

13. SUPPLEMENTARY NOTES

14. ABSTRACT

Using ground target radar tracks as building blocks, sophisticated road map estimation and fusion algorithms are developed. A maximum likelihood road estimator, as well as its corresponding Cramer-Rao lower bound, is derived. A track to road association approach is developed to align track segments to existing road segments. If a track is associated to any existing road segment, a track to road fusion algorithm is proposed to fuse the track with the corresponding road segment to improve the road map accuracy; otherwise, a new road is added to the road network. Numerical results are provided to demonstrate the effectiveness of the proposed road estimation and fusion approach.

15. SUBJECT TERMS
Road Networks, Estimation, Classification, Radar Tracks, GMTI Tracks

16. SECURITY CLASSIFICATION OF:			17. LIMITATION OF ABSTRACT	18. NUMBER OF PAGES	19a. NAME OF RESPONSIBLE PERSON
a. REPORT	b. ABSTRACT	c. THIS PAGE			**ADNAN BUBALO**
U	U	U	UU	33	19b. TELEPHONE NUMBER (*Include area code*) **N/A**

Table of Contents

List of Figures

List of Tables

1 SUMMARY

The goal of this project is the development of sophisticated road map extraction and fusion algorithms which use the ground target radar tracks as building blocks. We develop innovative frameworks, methodologies and algorithms that intelligently fuse tracks of different targets which move along the same road over time, to obtain accurate and refined estimate of the road map.

In this project, modeling the roads as piecewise linear segments, an appropriate data structure is developed to represent the road network map. An maximum likelihood (ML) road estimator using radar tracks, as well as its corresponding Cramér-Rao lower bound (CRLB), is derived. To properly fuse target tracks with the road network, a track to road correlation/association approach is proposed to align track segments to existing road segments. To enhance the association performance, statistics and information extracted from the track estimate, including both position and velocity estimates, are used in the track to road association approach. If the track has overlap with any existing road segments, a track to road fusion algorithm is proposed to fuse the track with the associated road segments to improve the road map accuracy; otherwise, a new road is added to the road network based on the target track. This process is repeated till all the available radar tracks are integrated/fused with the radar map. In this project, we derive theoretical results for road estimation based on radar tracks, track to road association, road to road association, and road fusion. Numerical results are provided to demonstrate the effectiveness of the proposed road estimation and fusion approaches.

2 INTRODUCTION

In this project, we seek to extract road maps based on ground vehicle tracks which are estimated using radar measurements, such as those obtained from the ground moving target indicator (GMTI). Accurate and up-to-date roadmaps are crucial for many purposes such as navigation, target tracking [1, 2], and airborne knowledge-aided space-time adaptive processing (STAP) [3, 4]. Digital road maps produced by the National Imagery and Mapping Agency (NIMA) as well as the United States Geological Survey (USGS), the two most common sources of such maps, often have errors that are large compared to the resolution of the GMTI sensors [5]. Road maps may be manually extracted from aerial photographs or synthetic aperture radar (SAR) images, but this process is extremely slow and laborious. Automatic transformation of images into digital road maps is possible, but is a difficult task and prone to errors, such as the false roads caused by boundaries in the image. As a result, radar track-driven road map extraction is an important and challenging problem in scenarios where road maps are not available, or where they are not sufficiently accurate or up-to-date.

2.1 Literature Review

2.1.1 Road Map Extraction from GMTI Data

A literature search has been conducted for road map conflation using radar data. There are a few publications on the topic of road map extraction based on GMTI data. In [5], O'Neil modeled the road itself as a trajectory through space, which is indexed by arc-length instead of by time. An iterative procedure to estimate the road using GMTI data was proposed, which starts with the initial knowledge of the road trajectory estimate provided by target tracking algorithms.

Koch et al. [6] applied track smoothing techniques to improve the target trajectory estimates, which are used to build the road map. The road map information was further employed to assist tracking of targets that move along the roads.

In [7], Sklarz et al. deemed track and the road as composite curve entities rather than sequences of points, which were associated and fused as a whole. In [7], by using dynamical time warping (DTW), similarity measures are proposed to measure the distance between two curves, which facilitate the track to road association process. The track to road fusion problem was cast as a curve fusion problem and a preliminary curve to curve fusion approach was developed by simply fusing matched points and ignoring the unknown correlation between the road estimation error and the track estimation error.

2.1.2 Road Map Extraction from Images

Some recently published papers are related to the road network conflation problem using image data [8,9]. In [8], the authors proposed to extract road intersections and terminations from imagery based on spatial contextual measures. The extracted intersections were used as control points for conflation algorithm. In [9], an EKF has been combined with a special particle filter to regain the trace of the road beyond obstacles, as well as to find and follow different road branches after reaching to a road junction.

2.2 Background in Track to Road Association

Track to road association is a very crucial step in the road map generation. Here we first study the hypothesis testing problem to determine whether the target state estimate at a particular time belongs to an exiting road segment or not. Below, we present three approaches based on the normalized distance (Mahalanobis distance), likelihood with diffuse prior, and the generalized likelihood and discuss the relationship between the first two.

2.2.1 Traditional Track-to-Track Association

A straightforward way for track-to-road association (correlation) is to utilize the position estimates contained in the target tracks. More specifically, similar to the track to track association approach in [10], we propose the following hypothesis test to decide whether

a target at a certain time is on the existing roads or not. First, let $\mathbf{x}_k$ denote the target position estimate at time k with a covariance matrix $\mathbf{P}_k$, and $\mathbf{x}_l$ denote the position estimate of an arbitrary point on the existing roads in the road map with a covariance matrix $\mathbf{P}_l$. For simplicity, we assume that $\mathbf{x}_k$ and $\mathbf{x}_l$ are jointly Gaussian with cross-covariance matrices $\mathbf{P}_{kl} = \mathbf{P}_{lk}^T$. We define the difference between these two position estimates as

$$\Delta_{kl} = \mathbf{x}_k - \mathbf{x}_l \tag{1}$$

If both $\mathbf{x}_k$ and $\mathbf{x}_l$ are unbiased estimates and they correspond to the same location, then Δ_{kl} follows a Gaussian distribution with zero mean and covariance matrix $\mathbf{P}_k+\mathbf{P}_l-\mathbf{P}_{kl}-\mathbf{P}_{lk}$. The point in the target track at time k can be associated to the existing roads by testing the following statistic:

$$d_1 = \min_l \left[\Delta_{kl}^T \left(\mathbf{P}_k + \mathbf{P}_l - \mathbf{P}_{kl} - \mathbf{P}_{lk}\right)^{-1} \Delta_{kl}\right] \tag{2}$$

Note that the search space of the above optimization problem can be significantly reduced, if a gating procedure is used to prune the existing road points which are clearly not associated with $\mathbf{x}_k$.

If $\mathbf{x}_k$ belongs to an exiting road, d_1 follows a Chi-square distribution with n_x degrees of freedom, where n_x is the dimension of the target position vector, which is three when the road is represented in a three-dimensional space. For a pre-specified probability of type I error α , the test threshold can be obtained as

$$T_\alpha = F_{\chi^2_{n_x}}^{-1}(1-\alpha) \tag{3}$$

where $F_{\chi^2_3}^{-1}$ is the inverse of the cumulative distribution function of a Chi-square distributed random variable with n_x degrees of freedom. When $d_1 < T_\alpha$, we can decide that the point belongs to the existing roads.

2.2.2 Likelihood with Diffuse Prior

In [11], under the assumption that the prior of the true target state $\mathbf{x}$ is a Gaussian distribution with an arbitrary mean μ and scaled covariance $\sigma^2\mathbf{P}$, Kaplan et al. showed that as $\sigma^2 \to \infty$, the likelihood of two tracks, $\mathbf{x}_k$ and $\mathbf{x}_l$, corresponding to the same target state $\mathbf{x}$, becomes

$$L(\mathbf{x}_k, \mathbf{x}_l) = \frac{1}{\left|2\pi\left(\mathbf{P}_k + \mathbf{P}_l - \mathbf{P}_{kl} - \mathbf{P}_{lk}\right)\right|^{\frac{1}{2}}} \exp\left[-\frac{1}{2}\Delta_{kl}^T \left(\mathbf{P}_k + \mathbf{P}_l - \mathbf{P}_{kl} - \mathbf{P}_{lk}\right)^{-1} \Delta_{kl}\right] \tag{4}$$

Therefore, a proper test statistic is obtained in a straightforward manner as follows

$$d_2 = \min_l \left[\log\left|2\pi\left(\mathbf{P}_k + \mathbf{P}_l - \mathbf{P}_{kl} - \mathbf{P}_{lk}\right)\right| + \Delta_{kl}^T \left(\mathbf{P}_k + \mathbf{P}_l - \mathbf{P}_{kl} - \mathbf{P}_{lk}\right)^{-1} \Delta_{kl}\right] \tag{5}$$

Comparing d_2 in (5) with d_1 in (2), it is clear that they are almost the same, except that in d_2, an extra penalty term has been introduced to favor those associations resulting smaller covariance matrix $(\mathbf{P}_k + \mathbf{P}_l - \mathbf{P}_{kl} - \mathbf{P}_{lk})$.

2.2.3 Generalized Likelihood

If the target state estimate can be treated as a deterministic vector, one can use the generalized likelihood approach [11]. Given the target state $\mathbf{x}$ is known, the likelihood of $\mathbf{x}_k$ and $\mathbf{x}_l$ is

$$L(\mathbf{x}_k, \mathbf{x}_l|\mathbf{x}) = \frac{1}{|2\pi\Sigma|^{\frac{1}{2}}} \exp\left[-\frac{1}{2}\left(\mathbf{x}_2 - \mathbf{I}_2\mathbf{x}\right)^T \Sigma^{-1}\left(\mathbf{x}_2 - \mathbf{I}_2\mathbf{x}\right)\right] \tag{6}$$

where $\mathbf{x}_2 = [\mathbf{x}_k^T\ \mathbf{x}_l^T]^T$, $\mathbf{I}_2 = [\mathbf{I}_{n_x\times n_x}\ \mathbf{I}_{n_x\times n_x}]^T$ and

$$\Sigma = \begin{bmatrix} \mathbf{P}_k & \mathbf{P}_{kl} \\ \mathbf{P}_{lk} & \mathbf{P}_l \end{bmatrix}$$

Since $\mathbf{x}$ is unknown, in a generalized likelihood, it is replaced by its ML estimate based on $\mathbf{x}_k$ and $\mathbf{x}_l$, which is the fused state estimate $\mathbf{x}_f$. It is well known that the fused state $\mathbf{x}_f$ is

$$\mathbf{x}_f = \mathbf{P}_f\ \mathbf{I}_2^T\Sigma^{-1}\mathbf{x}_2 \tag{7}$$

where

$$\mathbf{P}_f = \left(\mathbf{I}_2^T\Sigma^{-1}\mathbf{I}_2\right)^{-1} \tag{8}$$

Therefore, the GL is given as follows

$$\begin{aligned} L(\mathbf{x}_k, \mathbf{x}_l|\mathbf{x}) &= \frac{1}{|2\pi\Sigma|^{\frac{1}{2}}} \exp\left[-\frac{1}{2}\left(\mathbf{x}_2 - \mathbf{I}_2\mathbf{x}_f\right)^T \Sigma^{-1}\left(\mathbf{x}_2 - \mathbf{I}_2\mathbf{x}_f\right)\right] \\ &= \frac{1}{|2\pi\Sigma|^{\frac{1}{2}}} \exp\left[-\frac{1}{2}\left(\mathbf{x}_2^T\Sigma^{-1}\mathbf{x}_2 - \mathbf{x}_f^T\mathbf{P}_f^{-1}\mathbf{x}_f\right)\right] \end{aligned} \tag{9}$$

As a result, the test statistic based on the GL is

$$d_3 = \min_l \left[\log|2\pi\Sigma| + \left(\mathbf{x}_2^T\Sigma^{-1}\mathbf{x}_2 - \mathbf{x}_f^T\mathbf{P}_f^{-1}\mathbf{x}_f\right)\right] \tag{10}$$

3 METHODS, ASSUMPTIONS, AND PROCEDURES

3.1 Conversion between Different Coordinate Systems and Dataset Visualization

Matlab codes are developed for the conversion from geographic coordinates to topocentric coordinates, and for the display of the road map information.

In order to process the synthetic dataset, it is required to transform the coordinates of a target from the geographic coordinate system to the topocentric coordinate system. The earth is assumed to be an ellipsoid, and the geographic coordinates consist of latitude ϕ, longitude λ, and the ellipsoid height h of the target. A topocentric coordinate system is a 3-D Cartesian system having mutually perpendicular axes U, V, W with an origin on or

near the surface of the Earth. The U-axis is locally east, the V-axis is locally north and the W-axis is up forming a right-handed coordinate system.

For a given topocentric origin with the geographic coordinates ϕ_0, λ_0, and h_0, the conversion of a target's geographic coordinates $(\phi,\ \lambda,\ h)$ to its topocentric coordinates $(U,\ V,\ W)$, or the reverse formula to convert topocentric coordinates $(U,\ V,\ W)$ into latitude, longitude and ellipsoidal height $(\phi,\ \lambda,\ h)$, has been discussed in details in [12].

Based on the formulas described in [12], Matlab codes for the conversion from geographic coordinates to topocentric coordinates have been developed. Specifically, the earth is assumed to be an ellipsoid with the equatorial radius of 6378137.0 meters, and the polar radius of 6356752.314 meters. The Salt Flats of Utah are assumed to be 1286 meters above the sea level. The topocentric origin is taken as the center of the 10km $\times$ 10km area, with its latitude $\phi_0 = 40.7$ degrees, longitude $\lambda_0 = -113.875$ degrees, and the ellipsoid height $h_0 = 1286$ meters.

The truth data in SyntheticData.mat include the road segments, which are indicated by the geographic coordinates (latitude and longitude) of the starting and end way points. The Matlab program takes the truth data, converts the data to the topocentric coordinate system, and plots the road network in the topocentric coordinate system. In addition, the program also converts the track data from geographic coordinate system to topocentric coordinate system. In Figure 1, the map network and the first 5 target tracks in SyntheticData.mat have been plotted. It is clear that the tracks are very close to the corresponding roads, but they do not coincide with each other, due to estimation errors in the track data.

3.2 Road Conflation Based on Radar Positional Data

In this section, an efficient mathematical representation of the road is proposed, the likelihood function of the track data conditioned on the road parameters is derived, and solutions to road estimation based on track data, track to road association, road to road association, and road fusion are developed.

3.2.1 Road Representation

In the proposed approach, roads are represented by piece-wise linear segments. More particularly, a road is represented by the following straight line in the 2-D space:

$$y = ax + b \qquad x \in [\xi_s \ \ \xi_e] \tag{11}$$

where a is the slope, b the y-intercept. ξ_s and ξ_e are the x-coordinates of the start and end points of the road, respectively. The problem of road estimation is to estimate the parameters, including a, b, ξ_s, and ξ_e, based on the radar tracks.

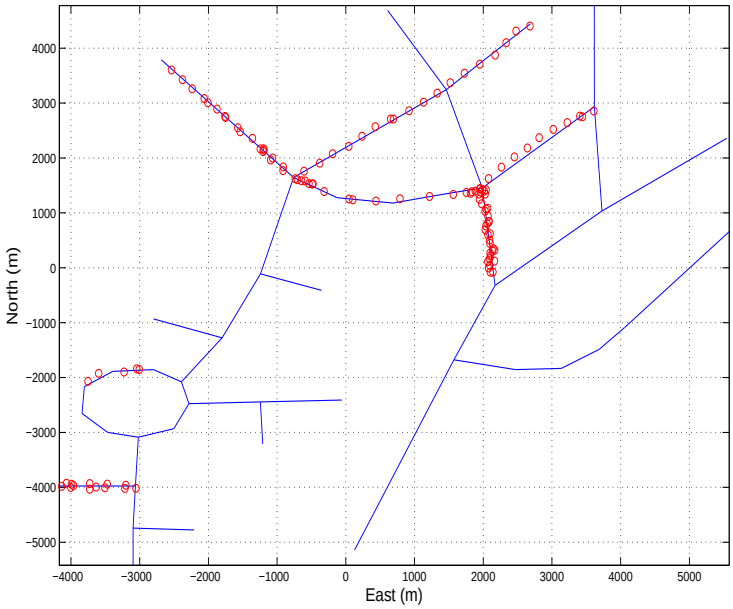

Figure 1: Road network and the first five tracks in SyntheticData.mat. Solid lines: roads; circles: tracks.

3.2.2 Likelihood of Track Data

Let us assume that a segment of track, which corresponds to the same road, consists of N data points:

$$\begin{aligned} \mathbf{z}_{1:N} &= [\hat{x}_1,\ \hat{y}_1,\ \cdots,\ \hat{x}_N,\ \hat{y}_N]^T \\ &= [\mathbf{z}_1^T,\ \cdots,\ \mathbf{z}_N^T]^T \end{aligned} \tag{12}$$

where $\mathbf{z}_i \triangleq [\hat{x}_i,\ \hat{y}_i]^T$ is the estimate of the x and y coordinates of the target at time i, whose estimation error covariance is denoted as $\mathbf{\Sigma}_i$. Further, the parameters of the estimation problem are denoted as $\mathbf{s} = [x_1,\ x_2,\ \cdots,\ x_N,\ a,\ b]^T$. With these notations and assumptions, the likelihood of $\mathbf{z}_{1:N}$ can be derived as

$$p(\mathbf{z}_{1:N}|\mathbf{s}) = \prod_{i=1}^{N} \frac{1}{|2\pi\Sigma_i|^{\frac{1}{2}}} e^{-\frac{(\mathbf{z}_i-\boldsymbol{\mu}_i)^T\Sigma_i^{-1}(\mathbf{z}_i-\boldsymbol{\mu}_i)}{2}} \tag{13}$$

where $\boldsymbol{\mu}_i = [x_i\ ax_i + b]^T$. The corresponding log-likelihood is

$$\log p(\mathbf{z}_{1:N}|\mathbf{s}) = \sum_{i=1}^{N} -\frac{(\mathbf{z}_i - \boldsymbol{\mu}_i)^T\Sigma_i^{-1}(\mathbf{z}_i - \boldsymbol{\mu}_i)}{2} + c \tag{14}$$

where c is a constant independent of $\mathbf{s}$.

3.2.3 Maximum Likelihood Estimation of Road

The maximum likelihood estimator (MLE) of $\mathbf{s}$ is therefore

$$\hat{\mathbf{s}} = \arg\min_{\mathbf{s}} \sum_{i=1}^{N} (\mathbf{z}_i - \boldsymbol{\mu}_i)^T \Sigma_i^{-1} (\mathbf{z}_i - \boldsymbol{\mu}_i) \tag{15}$$

We derive the MLE of $\mathbf{s}$ and summarize it in the following theorem.

Theorem 1 *The optimal MLE of* $\mathbf{s}$ *based on position information in radar tracks is a two-step procedure. First, the estimate of* x_i*, denoted as* $\hat{\xi}_i$*, should satisfy the following condition*

$$\hat{\xi}_i = -\frac{\mathbf{c}^T \Sigma_i^{-1} \mathbf{d_i}}{\mathbf{c}^T \Sigma_i^{-1} \mathbf{c}} \qquad \forall\ i \tag{16}$$

where $\mathbf{c} = [1 \quad a]^T$ *and* $\mathbf{d}_i = [-\hat{x}_i \quad b - \hat{y}_i]^T$*. Plugging (16) back into (15), the MLE of* $\boldsymbol{\eta} = [a \ \ b]^T$ *is*

$$\hat{\boldsymbol{\eta}} = \arg\min_{\boldsymbol{\eta}} \sum_{i=1}^{N} \mathbf{d}_i^T \Sigma_i^{-1} \mathbf{d_i} - \frac{\left(\mathbf{c}^T \Sigma_i^{-1} \mathbf{d_i}\right)^2}{\mathbf{c}^T \Sigma_i^{-1} \mathbf{c}} \tag{17}$$

Proof: First, we re-write the cost function in (15) as

$$\begin{aligned} \sum_{i=1}^{N} (\boldsymbol{\mu}_i - \mathbf{z}_i)^T \Sigma_i^{-1} (\boldsymbol{\mu}_i - \mathbf{z}_i) &= \sum_{i=1}^{N} (\mathbf{c}x_i + \mathbf{d}_i)^T \Sigma_i^{-1} (\mathbf{c}x_i + \mathbf{d}_i) \\ &= \sum_{i=1}^{N} \mathbf{c}^T \Sigma_i^{-1} \mathbf{c} x_i^2 + 2\mathbf{c}^T \Sigma_i^{-1} \mathbf{d}_i x_i + \mathbf{d}_i^T \Sigma_i^{-1} \mathbf{d}_i \end{aligned} \tag{18}$$

where the first equality follows from the identity

$$\begin{aligned} \boldsymbol{\mu}_i - \mathbf{z}_i &= [x_i - \hat{x}_i \quad a x_i + b - \hat{y}_i]^T \\ &= [1 \quad a]^T x_i + [-\hat{x}_i \quad b - \hat{y}_i]^T \\ &= \mathbf{c}x_i + \mathbf{d}_i \end{aligned} \tag{19}$$

Since the ith element in the summation in (18) is only a quadratic function of x_i, $\hat{\xi}_i$, the optimal estimator of x_i, must satisfy the following condition

$$\hat{\xi}_i = -\frac{\mathbf{c}^T \Sigma_i^{-1} \mathbf{d_i}}{\mathbf{c}^T \Sigma_i^{-1} \mathbf{c}} \tag{20}$$

Substituting this condition back into (18), we finally have

$$\sum_{i=1}^{N} \mathbf{d}_i^T \Sigma_i^{-1} \mathbf{d_i} - \frac{\left(\mathbf{c}^T \Sigma_i^{-1} \mathbf{d_i}\right)^2}{\mathbf{c}^T \Sigma_i^{-1} \mathbf{c}} \tag{21}$$

Therefore, the MLE of $\boldsymbol{\eta}$ is (17), and the MLE of x_i is

$$\hat{\xi}_i = -\frac{\mathbf{c}(\hat{\boldsymbol{\eta}})^T \Sigma_i^{-1} \mathbf{d_i}(\hat{\boldsymbol{\eta}})}{\mathbf{c}(\hat{\boldsymbol{\eta}})^T \Sigma_i^{-1} \mathbf{c}(\hat{\boldsymbol{\eta}})} \tag{22}$$

Q.E.D.

Note that Theorem 1 simplifies the MLE, an optimization problem, significantly when N is large. The original MLE problem as defined in (15) involves optimization in a $(N+2)$-dimensional search space, whereas the optimization problem in Theorem 1 requires a search in merely a 2-dimensional space.

We also derive the Cramér-Rao lower bound (CRLB) on the estimation error covariance matrix for any unbiased estimator of $\boldsymbol{\eta}$, which is provided in the following theorem.

Theorem 2 *The Fisher information matrix* $\mathbf{F}$*, which is the inverse of the CRLB matrix, for estimating* $\boldsymbol{\eta}$ *is*

$$\mathbf{F} = \sum_{i=1}^{N} \mathbf{E}_i - \mathbf{G}_i \tag{23}$$

where

$$\mathbf{E}_i = \begin{bmatrix} \mathbf{e}_i^T \Sigma_i^{-1} \mathbf{e}_i & \mathbf{e}_i^T \Sigma_i^{-1} \mathbf{f} \\ \mathbf{e}_i^T \Sigma_i^{-1} \mathbf{f} & \mathbf{f}^T \Sigma_i^{-1} \mathbf{f} \end{bmatrix} \tag{24}$$

$$\mathbf{G}_i = \frac{1}{\mathbf{c}^T \Sigma_i^{-1} \mathbf{c}} \begin{bmatrix} \left(\mathbf{c}^T \Sigma_i^{-1} \mathbf{e}_i\right)^2 & \left(\mathbf{c}^T \Sigma_i^{-1} \mathbf{e}_i\right)\left(\mathbf{c}^T \Sigma_i^{-1} \mathbf{f}\right) \\ \left(\mathbf{c}^T \Sigma_i^{-1} \mathbf{e}_i\right)\left(\mathbf{c}^T \Sigma_i^{-1} \mathbf{f}\right) & \left(\mathbf{c}^T \Sigma_i^{-1} \mathbf{f}\right)^2 \end{bmatrix} \tag{25}$$

$\mathbf{e}_i = [0 \;\; x_i]^T$*, and* $\mathbf{f} = [0 \;\; 1]^T$*.*

Proof: Let us denote $L = \log p(\mathbf{z}_{1:N}|\mathbf{s})$, then the Fisher information matrix (FIM) $\mathbf{J}$ for estimating $\mathbf{s}$ is

$$\mathbf{J} = E\{\nabla_{\mathbf{s}} L \; \nabla_{\mathbf{s}}^T L\} \tag{26}$$

Using (14), we have

$$\begin{aligned} \frac{\partial L}{\partial x_i} &= -\frac{1}{2} \sum_{j=1}^{N} \frac{\partial}{\partial x_i} \left[(\boldsymbol{\mu}_j - \mathbf{z}_j)^T \Sigma_j^{-1} (\boldsymbol{\mu}_j - \mathbf{z}_j) \right] \\ &= -\frac{1}{2} \sum_{j=1}^{N} \frac{\partial}{\partial x_i} \left\{ [x_j - \hat{x}_j \;\; a x_j + b - \hat{y}_j] \, \Sigma_j^{-1} \, [x_j - \hat{x}_j \;\; a x_j + b - \hat{y}_j]^T \right\} \\ &= -\frac{1}{2} \frac{\partial}{\partial x_i} \left\{ [x_i - \hat{x}_i \;\; a x_i + b - \hat{y}_i] \, \Sigma_i^{-1} \, [x_i - \hat{x}_i \;\; a x_i + b - \hat{y}_i]^T \right\} \\ &= -[1 \;\; a] \, \Sigma_i^{-1} \, [x_i - \hat{x}_i \;\; a x_i + b - \hat{y}_i]^T \end{aligned} \tag{27}$$

Let us define $\tilde{x}_i = x_i - \hat{x}_i$ and $\tilde{y}_i = ax_i + b - \hat{y}_i$. Then, it is easy to show that $[\tilde{x}_i \;\; \tilde{y}_i]^T$ has zero mean and covariance matrix Σ_i, and (27) can be re-written as

$$\frac{\partial L}{\partial x_i} = -\left[1 \;\; a\right] \Sigma_i^{-1} \left[\tilde{x}_i \;\; \tilde{y}_i\right]^T = -\mathbf{c}^T \; \Sigma_i^{-1} \left[\tilde{x}_i \;\; \tilde{y}_i\right]^T \tag{28}$$

Following a very similar procedure, we can prove the following

$$\frac{\partial L}{\partial a} = -\sum_{i=1}^{N} \left[0 \;\; x_i\right] \Sigma_i^{-1} \left[\tilde{x}_i \;\; \tilde{y}_i\right]^T = -\sum_{i=1}^{N} \mathbf{e}_i^T \Sigma_i^{-1} \left[\tilde{x}_i \;\; \tilde{y}_i\right]^T \tag{29}$$

and

$$\frac{\partial L}{\partial b} = -\sum_{i=1}^{N} \left[0 \;\; 1\right] \Sigma_i^{-1} \left[\tilde{x}_i \;\; \tilde{y}_i\right]^T = -\mathbf{f}^T \sum_{i=1}^{N} \Sigma_i^{-1} \left[\tilde{x}_i \;\; \tilde{y}_i\right]^T \tag{30}$$

Now we have

$$\begin{aligned} E\left\{\left(\frac{\partial L}{\partial x_i}\right)^2\right\} &= E\left\{\mathbf{c}^T \; \Sigma_i^{-1} \left[\tilde{x}_i \;\; \tilde{y}_i\right]^T \left[\tilde{x}_i \;\; \tilde{y}_i\right] \Sigma_i^{-1} \mathbf{c}\right\} \\ &= \mathbf{c}^T \; \Sigma_i^{-1} \mathbf{c} \end{aligned} \tag{31}$$

Similarly, we can prove that

$$E\left\{\frac{\partial L}{\partial x_i}\frac{\partial L}{\partial x_j}\right\} = 0 \quad \forall \; i \neq j \tag{32}$$

$$E\left\{\frac{\partial L}{\partial x_i}\frac{\partial L}{\partial a}\right\} = \mathbf{c}^T \; \Sigma_i^{-1} \mathbf{e}_i \tag{33}$$

$$E\left\{\frac{\partial L}{\partial x_i}\frac{\partial L}{\partial b}\right\} = \mathbf{c}^T \; \Sigma_i^{-1} \mathbf{f} \tag{34}$$

$$E\left\{\left(\frac{\partial L}{\partial a}\right)^2\right\} = \sum_{i=1}^{N} \mathbf{e}_i^T \; \Sigma_i^{-1} \mathbf{e}_i \tag{35}$$

$$E\left\{\left(\frac{\partial L}{\partial b}\right)^2\right\} = \sum_{i=1}^{N} \mathbf{f}^T \; \Sigma_i^{-1} \mathbf{f} \tag{36}$$

and

$$E\left\{\frac{\partial L}{\partial a}\frac{\partial L}{\partial b}\right\} = \sum_{i=1}^{N} \mathbf{e}_i^T \; \Sigma_i^{-1} \mathbf{f} \tag{37}$$

In summary, we have

$$\begin{aligned}
\mathbf{J} &= E\{\nabla_{\mathbf{s}} L \, \nabla_{\mathbf{s}}^T L\} \qquad (38)\\
&= \begin{bmatrix}
\mathbf{c}^T \Sigma_1^{-1}\mathbf{c} & 0 & \cdots & 0 & \mathbf{c}^T \Sigma_1^{-1}\mathbf{e}_1 & \mathbf{c}^T \Sigma_1^{-1}\mathbf{f} \\
0 & \mathbf{c}^T \Sigma_2^{-1}\mathbf{c} & \cdots & 0 & \mathbf{c}^T \Sigma_2^{-1}\mathbf{e}_2 & \mathbf{c}^T \Sigma_2^{-1}\mathbf{f} \\
\vdots & \vdots & \ddots & \vdots & \vdots & \vdots \\
0 & 0 & \cdots & \mathbf{c}^T \Sigma_N^{-1}\mathbf{c} & \mathbf{c}^T \Sigma_N^{-1}\mathbf{e}_N & \mathbf{c}^T \Sigma_N^{-1}\mathbf{f} \\
\mathbf{c}^T \Sigma_1^{-1}\mathbf{e}_1 & \mathbf{c}^T \Sigma_2^{-1}\mathbf{e}_2 & \cdots & \mathbf{c}^T \Sigma_N^{-1}\mathbf{e}_N & \sum_{i=1}^N \mathbf{e}_i^T \Sigma_i^{-1}\mathbf{e}_i & \sum_{i=1}^N \mathbf{e}_i^T \Sigma_i^{-1}\mathbf{f} \\
\mathbf{c}^T \Sigma_1^{-1}\mathbf{f} & \mathbf{c}^T \Sigma_2^{-1}\mathbf{f} & \cdots & \mathbf{c}^T \Sigma_N^{-1}\mathbf{f} & \sum_{i=1}^N \mathbf{e}_i^T \Sigma_i^{-1}\mathbf{f} & \sum_{i=1}^N \mathbf{f}^T \Sigma_i^{-1}\mathbf{f}
\end{bmatrix} \\
&= \begin{bmatrix} \mathbf{A} & \mathbf{B} \\ \mathbf{B}^T & \mathbf{D} \end{bmatrix}
\end{aligned}$$

where

$$\mathbf{A} = \begin{bmatrix}
\mathbf{c}^T \Sigma_1^{-1}\mathbf{c} & 0 & \cdots & 0 \\
0 & \mathbf{c}^T \Sigma_2^{-1}\mathbf{c} & \cdots & 0 \\
\vdots & \vdots & \ddots & \\
0 & 0 & \cdots & \mathbf{c}^T \Sigma_N^{-1}\mathbf{c}
\end{bmatrix} \qquad (39)$$

$$\mathbf{B}^T = \begin{bmatrix}
\mathbf{c}^T \Sigma_1^{-1}\mathbf{e}_1 & \mathbf{c}^T \Sigma_2^{-1}\mathbf{e}_2 & \cdots & \mathbf{c}^T \Sigma_N^{-1}\mathbf{e}_N \\
\mathbf{c}^T \Sigma_1^{-1}\mathbf{f} & \mathbf{c}^T \Sigma_2^{-1}\mathbf{f} & \cdots & \mathbf{c}^T \Sigma_N^{-1}\mathbf{f}
\end{bmatrix} \qquad (40)$$

and

$$\mathbf{D} = \begin{bmatrix}
\sum_{i=1}^N \mathbf{e}_i^T \Sigma_i^{-1}\mathbf{e}_i & \sum_{i=1}^N \mathbf{e}_i^T \Sigma_i^{-1}\mathbf{f} \\
\sum_{i=1}^N \mathbf{e}_i^T \Sigma_i^{-1}\mathbf{f} & \sum_{i=1}^N \mathbf{f}^T \Sigma_i^{-1}\mathbf{f}
\end{bmatrix} \qquad (41)$$

The CRLB matrix $\mathbf{C}_c$ for estimating $\mathbf{s}$ is

$$\mathbf{C}_c = \mathbf{J}^{-1} = \begin{bmatrix} \mathbf{A} & \mathbf{B} \\ \mathbf{B}^T & \mathbf{D} \end{bmatrix}^{-1} \qquad (42)$$

Using blockwise matrix inversion [13], we know that the lower right 2×2 sub-matrix corresponding to the estimation of $\boldsymbol{\eta} = [a \;\; b]^T$ is $\left(\mathbf{D} - \mathbf{B}^T\mathbf{A}^{-1}\mathbf{B}\right)^{-1}$. As a result, the FIM for estimating $\boldsymbol{\eta}$ is simply

$$\mathbf{F} = \mathbf{D} - \mathbf{B}^T\mathbf{A}^{-1}\mathbf{B} \qquad (43)$$

Plugging (39), (40), and (41) into (43), we can finally prove the theorem. Q.E.D.

From Theorem 2, it is clear that complexity in calculating $\mathbf{F}$ is significantly reduced when N is large. The calculation of $\mathbf{F}$ involves the inverse of matrices with smaller dimensions (2×2), instead of the inverse of the original $(N+2) \times (N+2)$ FIM $\mathbf{J}$ for $\mathbf{s}$.

3.2.4 Track to Road Association

To test whether or not a track data point $\mathbf{z} = [\hat{x} \; \hat{y}]^T$ with covariance matrix Σ belongs to a particular road with parameter estimate $\hat{\boldsymbol{\eta}} = [\hat{a} \; \hat{b}]^T$ and covariance matrix $\Sigma_{\boldsymbol{\eta}}$, a Chi-square test is adopted.

First, denote $\Delta_1 = \hat{y} - (\hat{a}\hat{x} + \hat{b})$. Then, it can be shown that

$$E[\Delta_1] = 0 \quad (44)$$

$$\text{Var}[\Delta_1] = \mathbf{g}^T \Sigma\, \mathbf{g} + \mathbf{h}^T \Sigma_{\boldsymbol{\eta}} \mathbf{h} + \Sigma_{\boldsymbol{\eta}}(1,1) \times \Sigma(1,1) \quad (45)$$

As a result, the test statistic is set as $\frac{\Delta_1^2}{\text{Var}[\Delta_1]}$, which given a Gaussian assumption, follows a Chi-square distribution with 1 degree of freedom. Hence, if $\frac{\Delta_1^2}{\text{Var}[\Delta_1]} \leq t_1$, then $\mathbf{z}$ belongs to the road parameterized by $\hat{\boldsymbol{\eta}}$, where t_1 is a pre-defined threshold which can be determined by a pre-specified probability of type I error.

3.2.5 Road to Road Association

To test whether or not a road estimate $\hat{\boldsymbol{\eta}}_1$ with covariance matrix Σ_1 can be associated with another road estimate $\hat{\boldsymbol{\eta}}_2$ with covariance matrix Σ_2, a similar Chi-square test can be adopted.

First, denote $\boldsymbol{\Delta}_2 = \hat{\boldsymbol{\eta}}_1 - \hat{\boldsymbol{\eta}}_2$. Then, it can be shown that

$$E[\Delta_2] = \mathbf{0} \quad (46)$$

$$\text{Cov}[\boldsymbol{\Delta}_2] = \Sigma_1 + \Sigma_2 \quad (47)$$

As a result, the test statistic is set as $\boldsymbol{\Delta}_2^T (\Sigma_1 + \Sigma_2)^{-1} \boldsymbol{\Delta}_2$, which given a Gaussian assumption, follows a Chi-square distribution with 2 degrees of freedom. Hence, if $\boldsymbol{\Delta}_2^T (\Sigma_1 + \Sigma_2)^{-1} \boldsymbol{\Delta}_2 \leq t_2$, then these two road estimates can be taken as to correspond to the same road. t_2 is a pre-defined threshold which can be determined by a pre-specified probability of type I error.

3.2.6 Road Fusion

If a road estimate $\hat{\boldsymbol{\eta}}_1$ with covariance matrix Σ_1 can be associated with another road estimate $\hat{\boldsymbol{\eta}}_2$ with covariance matrix Σ_2, they should be fused to get a more accurate road estimate.

The fused road estimate is

$$\hat{\boldsymbol{\eta}} = \Sigma_2 (\Sigma_1 + \Sigma_2)^{-1} \hat{\boldsymbol{\eta}}_1 + \Sigma_1 (\Sigma_1 + \Sigma_2)^{-1} \hat{\boldsymbol{\eta}}_2 \quad (48)$$

and the corresponding covariance matrix of the fused estimate is

$$\Sigma = \Sigma_2 (\Sigma_1 + \Sigma_2)^{-1} \Sigma_1 \quad (49)$$

3.3 Road Conflation Based on Both Radar Positional and Velocity Data

In Section 3.2, only position estimates in the radar tracks were used for road network estimation. The velocity estimates, which also contain valuable information about the roads (especially that about the directions of the roads), were not employed. In this section, a road estimation approach is developed to incorporate both position and velocity information in the radar track data. The maximum likelihood estimator (MLE) of a road based on radar tracks and its corresponding Cramér-Rao lower bound matrix are derived.

3.3.1 Likelihood of Track Data

As in Section 3.2, roads are represented by piece-wise linear segments, which are modeled by straight lines in the 2-D space with slope a and y-intercept b. It is reasonable to assume that the target moves towards the same direction as that defined by the current road segment, except when it makes turns at road intersections. Hence, we have

$$v_y = a v_x \tag{50}$$

where v_x and v_y are the target velocities along the x and y axes, respectively.

Let us assume that a segment of track, which corresponds to the same road, consists of N data points:

$$\begin{aligned} \mathbf{z}_{1:N} &= [\hat{x}_1,\ \hat{y}_1,\ \hat{v}_{x_1},\ \hat{v}_{y_1},\ \cdots,\ \hat{x}_N,\ \hat{y}_N,\ \hat{v}_{x_N},\ \hat{v}_{y_N}]^T \\ &= [\mathbf{z}_1^T,\ \cdots,\ \mathbf{z}_N^T]^T \end{aligned} \tag{51}$$

where $\mathbf{z}_i \triangleq [\hat{x}_i,\ \hat{y}_i,\ \hat{v}_{x_i},\ \hat{v}_{y_i}]^T$ is the state estimate of the target at time i, which consists of the estimates of the target position and velocity along x and y axes, respectively. The estimation error covariance matrix is denoted as $\mathbf{\Sigma}_i$. Further, the parameters of the estimation problem are denoted as $\mathbf{s} = [x_1,\ v_{x_1},\ x_2,\ v_{x_2}, \cdots,\ x_N,\ v_{x_N},\ a,\ b]^T$. With these notations and assumptions, the likelihood of $\mathbf{z}_{1:N}$ can be derived as

$$p(\mathbf{z}_{1:N}|\mathbf{s}) = \prod_{i=1}^{N} \frac{1}{|2\pi\Sigma_i|^{\frac{1}{2}}} e^{-\frac{(\mathbf{z}_i-\boldsymbol{\mu}_i)^T\Sigma_i^{-1}(\mathbf{z}_i-\boldsymbol{\mu}_i)}{2}} \tag{52}$$

where $\boldsymbol{\mu}_i = [x_i,\ ax_i + b,\ v_{x_i},\ av_{x_i}]^T$. The corresponding log-likelihood is

$$\log p(\mathbf{z}_{1:N}|\mathbf{s}) = \sum_{i=1}^{N} -\frac{(\mathbf{z}_i - \boldsymbol{\mu}_i)^T\Sigma_i^{-1}(\mathbf{z}_i - \boldsymbol{\mu}_i)}{2} + c \tag{53}$$

where c is a constant independent of $\mathbf{s}$.

3.3.2 Maximum Likelihood Estimation of Road

The Maximum Likelihood Estimation (MLE) of $\mathbf{s}$ is therefore

$$\hat{\mathbf{s}} = \arg\min_{\mathbf{s}} \sum_{i=1}^{N} (\mathbf{z}_i - \boldsymbol{\mu}_i)^T\Sigma_i^{-1}(\mathbf{z}_i - \boldsymbol{\mu}_i) \tag{54}$$

Analogous to Theorem 1, we derive a simplified version of the MLE as summarized in the following theorem.

Theorem 3 *The optimal MLE is a two-step procedure. For $1 \le i \le N$, let us denote $\mathbf{x}_i = [x_i,\ v_{x_i}]^T$. The estimate of $\mathbf{x}_i$, denoted as $\hat{\mathbf{x}}_i$, should stratify the following condition,*

$$\hat{\mathbf{x}}_i = -\left(\mathbf{C}^T\Sigma_i^{-1}\mathbf{C}\right)^{-1}\mathbf{C}^T\Sigma_i^{-1}\mathbf{m}_i \qquad \forall i \tag{55}$$

where

$$\mathbf{C} = \begin{bmatrix} 1 & 0 \\ a & 0 \\ 0 & 1 \\ 0 & a \end{bmatrix}$$

and

$$\mathbf{m}_i = [-\hat{x}_i,\ b - \hat{y}_i,\ -\hat{v}_{x_i},\ -\hat{v}_{y_i}]^T.$$

Plugging (55) back into (54), the MLE of $\boldsymbol{\eta} = [a,\ b]^T$ *is*

$$\hat{\boldsymbol{\eta}} = \arg\min_{\boldsymbol{\eta}} \sum_{i=1}^{N} \left[\mathbf{m}_i^T \Sigma_i^{-1} \mathbf{m}_i - \mathbf{m}_i^T \Sigma_i^{-1} \mathbf{C} \left(\mathbf{C}^T \Sigma_i^{-1} \mathbf{C} \right)^{-1} \mathbf{C}^T \Sigma_i^{-1} \mathbf{m}_i \right] \tag{56}$$

The proof of Theorem 3 is similar to that of Theorem 1, and is skipped here for brevity. Again, Theorem 3 simplifies the MLE problem significantly when N is large. The original MLE problem as defined in (54) involves optimization in a $(2N+2)$-dimensional search space, whereas the optimization problem in Theorem 3 requires a search in merely a 2-dimensional space.

The Fisher matrix $\mathbf{F}$ for estimating $\boldsymbol{s}$ is

$$\mathbf{F}_s = \begin{bmatrix} \Delta_1 & \mathbf{0} & \cdots & \mathbf{0} & \Delta_{1,\eta} \\ \mathbf{0} & \Delta_2 & \cdots & \mathbf{0} & \Delta_{2,\eta} \\ \vdots & \vdots & \ddots & \vdots & \vdots \\ \mathbf{0} & \mathbf{0} & \cdots & \Delta_N & \Delta_{N,\eta} \\ \Delta_{1,\eta}^T & \Delta_{2,\eta}^T & \cdots & \Delta_{N,\eta}^T & \Delta_\eta \end{bmatrix} \tag{57}$$

where

$$\Delta_i = \mathbf{C}^T \Sigma_i^{-1} \mathbf{C} \tag{58}$$

$$\Delta_{i,\eta} = \mathbf{C}^T \Sigma_i^{-1} \mathbf{D}_i \tag{59}$$

$$\Delta_\eta = \sum_{i-1}^{N} \mathbf{D}_i^T \Sigma_i^{-1} \mathbf{D}_i \tag{60}$$

are 2×2 sub-matrices, and

$$\mathbf{D}_i = \begin{bmatrix} 0 & 0 \\ x_i & 1 \\ 0 & 0 \\ v_{x_i} & 0 \end{bmatrix} \tag{61}$$

The CRLB matrix for estimating $\boldsymbol{\eta} = [a,\ b]^T$ can be obtained by first taking the inverse of the $(2N+2) \times (2N+2)$ $\mathbf{F_s}$ matrix, and then taking the lower-right 2×2 sub-matrix of $\mathbf{F_s}^{-1}$. However, this is not a very efficient approach especially when N is large and the inversion of a large $\mathbf{F_s}$ is involved. As we did in the proof of Theorem 2, taking advantage of the special structure of $\mathbf{F_s}$, and using blockwise matrix inversion [13], a much more efficient approach to calculate the Fisher information matrix $\mathbf{F}_\eta$ is derived and provided in the following theorem.

Theorem 4 *The Fisher information matrix for estimating η based on both position and velocity information in radar tracks is*

$$\mathbf{F}_\eta = \sum_{i=1}^{N} \left[\mathbf{D}_i^T \Sigma_i^{-1} \mathbf{D}_i - \mathbf{D}_i^T \Sigma_i^{-1} \mathbf{C} (\mathbf{C}^T \Sigma_i^{-1} \mathbf{C})^{-1} \mathbf{C}^T \Sigma_i^{-1} \mathbf{D}_i \right] \tag{62}$$

It is clear that the calculation of $\mathbf{F}_\eta$ only involves manipulation of matrices with smaller dimensions (such as 2×2, 4×2, 2×4, and 4×4.), instead of the original $(2N+2)\times(2N+2)$ matrix. Now, the CRLB matrix for estimating $\boldsymbol{\eta}$ can be readily obtained by taking the inverse of $\mathbf{F}_\eta$.

3.3.3 Track to Road Association Using both Position and Velocity Data

To associate a track data point $\mathbf{z} = [\hat{x}\ \hat{y}\ \hat{v}_x\ \hat{v}_y]^T$ with covariance matrix Σ to a road with parameter estimate $\hat{\boldsymbol{\eta}} = [\hat{a}\ \hat{b}]^T$ and covariance matrix $\Sigma_{\boldsymbol{\eta}}$, a Chi-square test is adopted. Assuming that $\mathbf{z}$ belongs to the road, we denote $\Delta_2 = [\hat{y} - (\hat{a}\hat{x} + \hat{b})\ \ \hat{v}_y - \hat{a}\hat{v}_x]^T$. Then, it can be shown that

$$E[\Delta_2] = \mathbf{0} \tag{63}$$

where $\mathbf{0}$ is a all-zero vector. The covariance matrix of Δ_2 is

$$\begin{aligned} \mathbf{\Sigma}_\Delta &= E\{\Delta_2 \Delta_2^T\} \\ &= \begin{bmatrix} \mathbf{f}^T\mathbf{\Sigma}\mathbf{f} + \mathbf{g}^T\mathbf{\Sigma}_\eta\mathbf{g} + \mathbf{\Sigma}(1,1)\mathbf{\Sigma}_\eta(1,1) & \mathbf{f}^T\mathbf{\Sigma}\mathbf{h} + \mathbf{g}^T\mathbf{\Sigma}_\eta\mathbf{k} + \mathbf{\Sigma}(1,3)\mathbf{\Sigma}_\eta(1,1) \\ \mathbf{f}^T\mathbf{\Sigma}\mathbf{h} + \mathbf{g}^T\mathbf{\Sigma}_\eta\mathbf{k} + \mathbf{\Sigma}(1,3)\mathbf{\Sigma}_\eta(1,1) & \mathbf{h}^T\mathbf{\Sigma}\mathbf{h} + \mathbf{k}^T\mathbf{\Sigma}_\eta\mathbf{k} + \mathbf{\Sigma}(3,3)\mathbf{\Sigma}_\eta(1,1) \end{bmatrix} \end{aligned} \tag{64}$$

in which

$$\mathbf{f} = [-\hat{a}\ 1\ 0\ 0]^T,\ \ \mathbf{h} = [0\ 0\ \ -\hat{a}\ 1]^T,\ \ \mathbf{g} = [-\hat{x}\ \ -1]^T,\ \ \mathbf{k} = [-\hat{v}_x\ 0]^T. \tag{65}$$

The test statistic, $t = \Delta_2^T \mathbf{\Sigma}_\Delta^{-1} \Delta_2$, follows a Chi-square distribution with 2 degrees of freedom. If $t \le t2$, then $\mathbf{z}$ belongs to the road parameterized by $\hat{\boldsymbol{\eta}}$, where t_2 is a pre-defined threshold corresponding to a pre-specified probability of type I error.

3.4 Overview of the Road Extraction Algorithm

Here we provide an overview of the road extract algorithm. Radar tracks are used as building blocks to generate road estimates. This is an iterative algorithm where a single radar trajectory is processed at each iteration. During each iteration, new road estimates will be either fused with exiting road estimates or added as new road. As more tracks are integrated into an initially empty map, the accuracy and richness of the map improve. A post processing algorithm can be applied to merge fragmented roads and prune isolated false roads. The overview of the algorithm is illustrated in Figure 2.

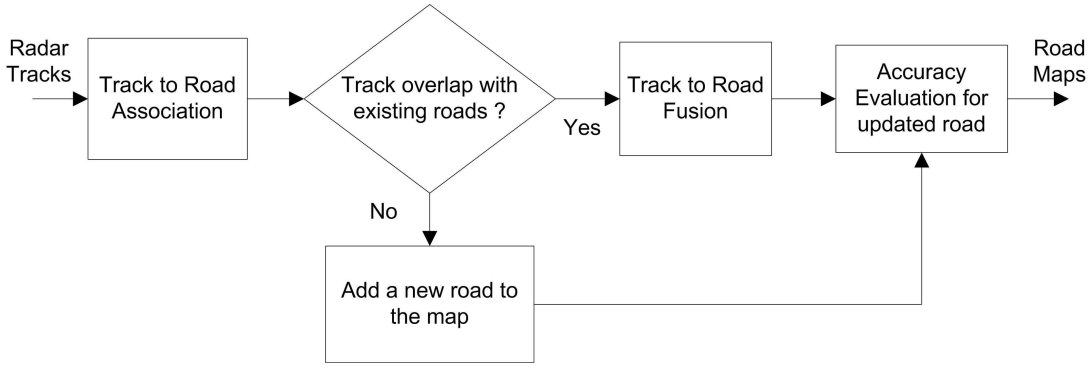

Figure 2: Road map extraction based on radar tracks.

4 RESULTS AND DISCUSSION

4.1 Numerical Examples based on Position Data Only

Based on the theoretical results derived in Section 3.2, we develop data structure for road representation, and Matlab codes for road estimation based on simulated radar tracks, track to road association, road to road association, and road fusion.

In Figure 3, a road estimation/extraction example is shown. The extracted roads are based on the first ten radar tracks. As shown in the figure, most of the time, the estimated roads are reasonably accurate and close to the underlying true road networks. However, for short road segments, the estimates sometimes are not very accurate. This is especially clear for part for the polygon circle in the lower-left corner of the figure.

In Figure 4, the road estimates based on all the radar tracks are presented. As shown in the figure, the estimated roads are most concentrated around the true roads. But there are a lot of fragmented roads and some false roads. To alleviate this problem, a post processing algorithm is applied to merge fragmented road estimates and eliminate isolated false road estimates. Road estimates after post processing (merging and pruning) are shown in Figure 5. It is clear that even after the post processing, the road estimates are still not ideal, and there still exist fragmented road estimates and false road estimates.

4.2 Numerical Examples Based on Both Position and Velocity Data

In Figure 6, a road estimation/extraction example is shown based on the first ten radar tracks, where both position and velocity information is used. As shown in the figure, most of the time, the estimated roads are reasonably accurate and close to the underlying true road networks. However, compared to Figure 3, there is an extra false road.

In Figure 7, the road estimates based on all the radar tracks are presented. As shown in the figure, the estimated roads are most concentrated around the true roads. But there

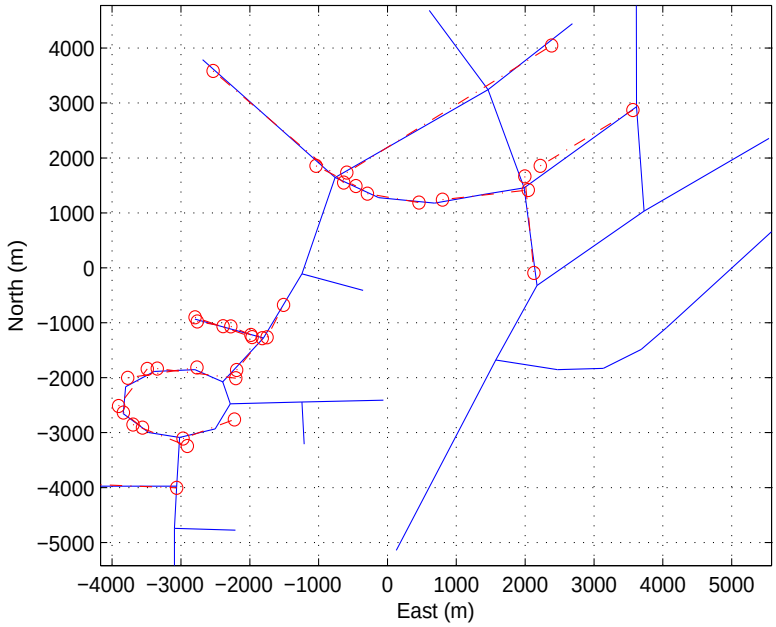

Figure 3: Estimated roads based on the first ten radar tracks. Blue solid lines: true roads; red dash-dot lines+circles: estimated roads.

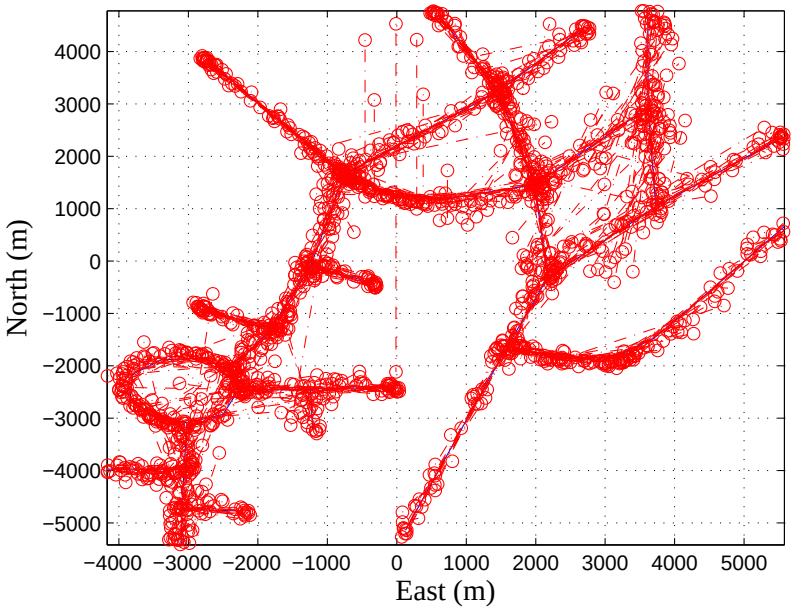

Figure 4: Estimated roads based on all radar tracks. Blue solid lines: true roads; red dash-dot lines+circles: estimated roads.

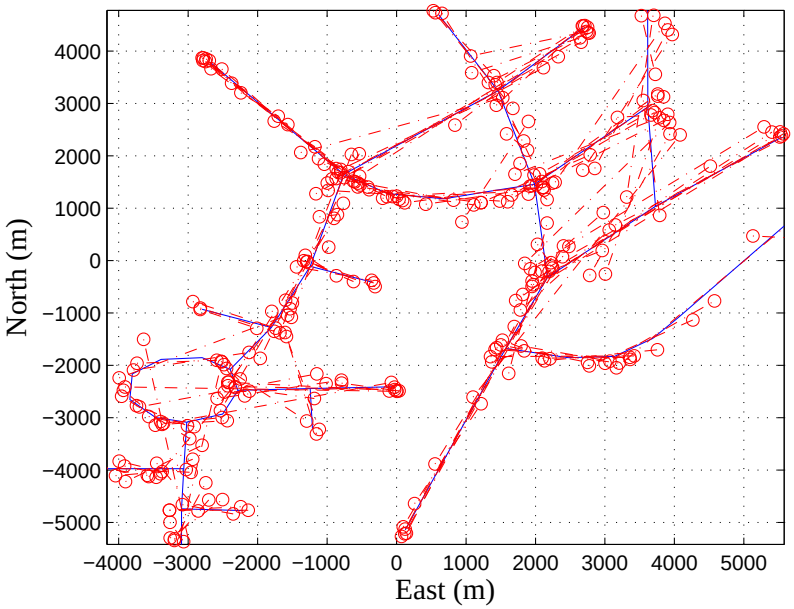

Figure 5: Estimated roads after pruning isolated road estimates. Blue solid lines: true roads; red dash-dot lines+circles: estimated roads.

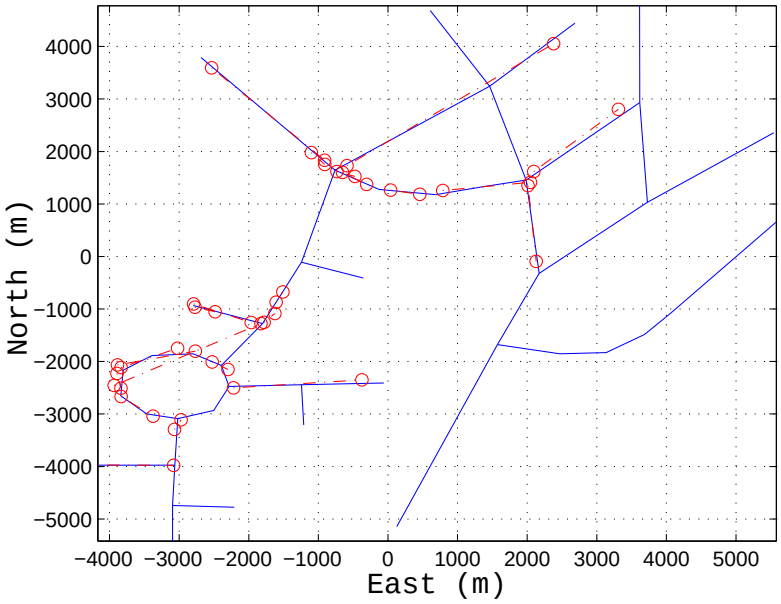

Figure 6: Estimated roads based on the first ten radar tracks. Blue solid lines: true roads; red dash-dot lines+circles: estimated roads.

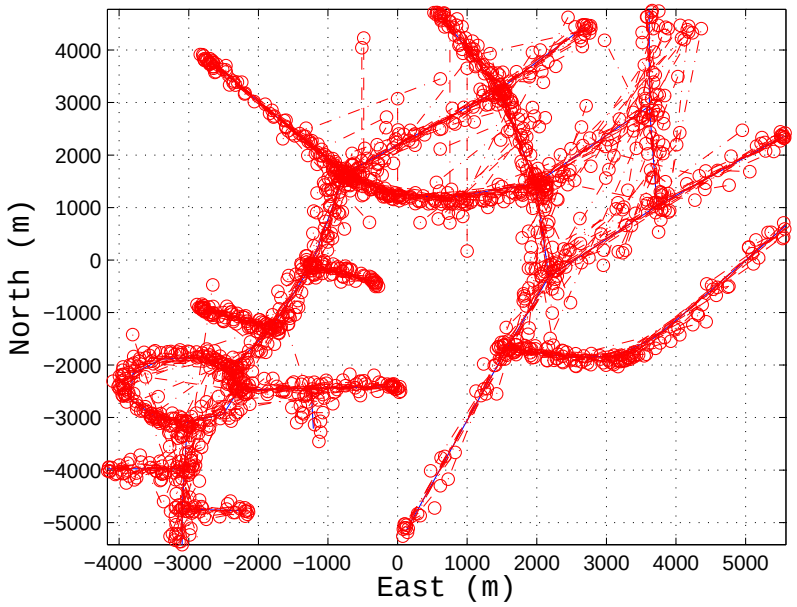

Figure 7: Estimated roads based on all radar tracks. Blue solid lines: true roads; red dash-dot lines+circles: estimated roads.

are a lot of fragmented roads and some false roads. To alleviate this problem, again a post processing algorithm is applied to merge fragmented road estimates and eliminate isolated false road estimates. Road estimates after post processing (merging and pruning) are shown in Figure 8. It is clear that even after the post processing, the road estimates are still not ideal, and there still exist fragmented road estimates and false road estimates. However, comparing Figure 5 and Figure 8, the estimation performance improvement achieved by using both position and velocity information is very clear.

4.3 Initialization using velocity data

From the experiments, it is found that the initialization of road estimate is very important and has direct impacts on the road estimation performance. So far in the initialization process, only radar track's position information has been used to estimate the road parameters a and b. Since the radar track's velocity data contain the road direction information, incorporation of this information has the potential to improve the road initialization, and to improve the following road estimation process. The following modification has been made to include the velocity information. Let us define the target's heading at time i as

$$\alpha_i = \text{atan2}(\hat{v}_{y_i},\ \hat{v}_{x_i})$$

where $\hat{v}_{x_i}$ and $\hat{v}_{y_i}$ are the target's velocity estimates along x and y axes at time i respectively. Two consecutive radar track data points at time i and $i+1$ are used to initialize a road

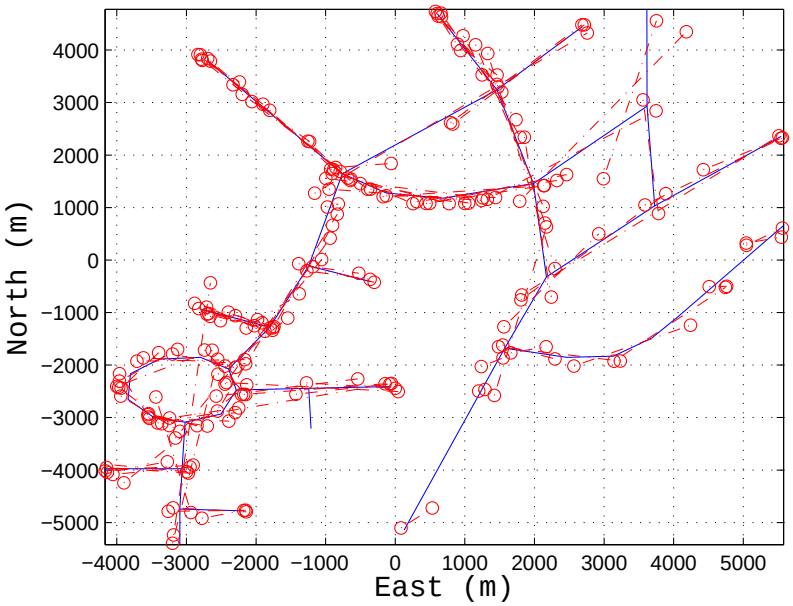

Figure 8: Estimated roads after pruning isolated road estimates. Blue solid lines: true roads; red dash-dot lines+circles: estimated roads.

estimate only if the two directions α_i and α_{i+1} are very close to each other. Mathematically, the condition is $|\alpha_i - \alpha_{i+1}| < \eta$, or $|\alpha_i + \pi - \alpha_{i+1}| < \eta$, or $|\alpha_i - \pi - \alpha_{i+1}| < \eta$, where η is a pre-specified threshold.

In this experiment, we set η as 5°. In Figures 9 and 10, the road estimates which are initialized without velocity information and those initialized with the velocity information are compared. It is clear that the latter provides us better road estimation solutions with less false roads.

4.4 Road Consistence Test

To further reduce the false road estimates, a road estimate consistence test is proposed. Once a new road estimate is generated, all the track data, which have been used to generate the road estimate, are subject to a track to road association procedure, as discussed in Section 3.3.3. If all the track data points passed the test, meaning that they are associated to the new road estimate, then the new road estimate is accepted and used to update the global road estimates; otherwise, the new road estimate does not have a good "match" with the track data and it is discarded. In this way, the possible false road estimates are removed from the road database.

In Figures 11 and 12, the algorithm involving road consistence tests is compared against that without the consistence test. It is clear that the former has much better performance with more consistent road estimates.

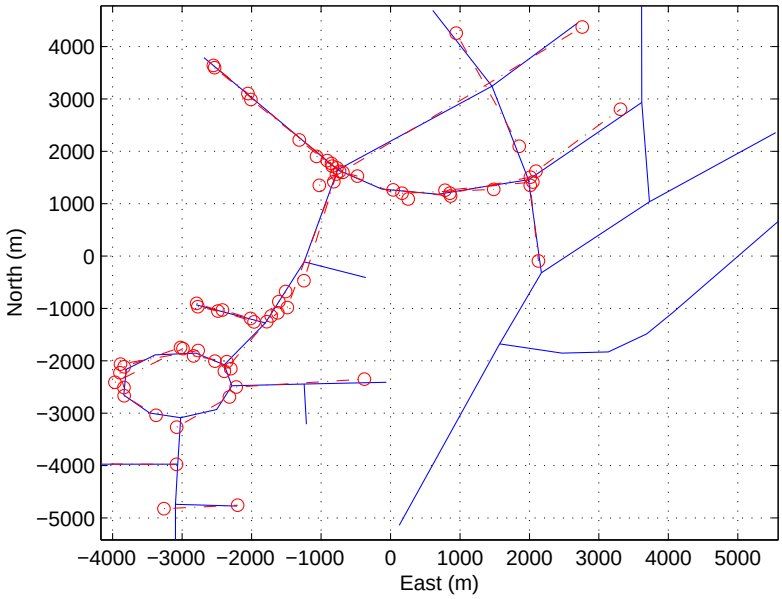

Figure 9: Estimated roads using the first 20 radar tracks. Roads are initialized without velocity data. Blue solid lines: true roads; red dash-dot lines+circles: estimated roads.

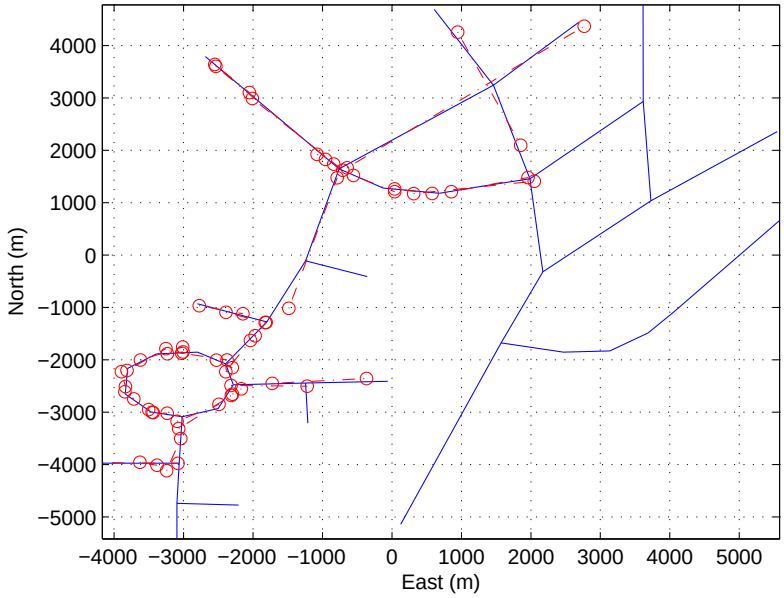

Figure 10: Estimated roads using the first 20 radar tracks. Roads are initialized with velocity data. Blue solid lines: true roads; red dash-dot lines+circles: estimated roads.

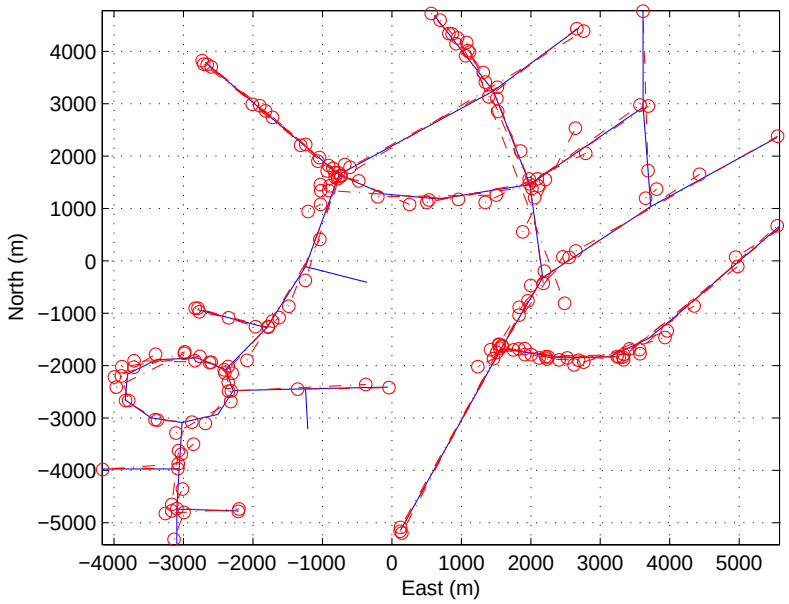

Figure 11: Estimated roads using the first 100 radar tracks without road consistence tests. A roads are initialized without velocity data. Blue solid lines: true roads; red dash-dot lines+circles: estimated roads.

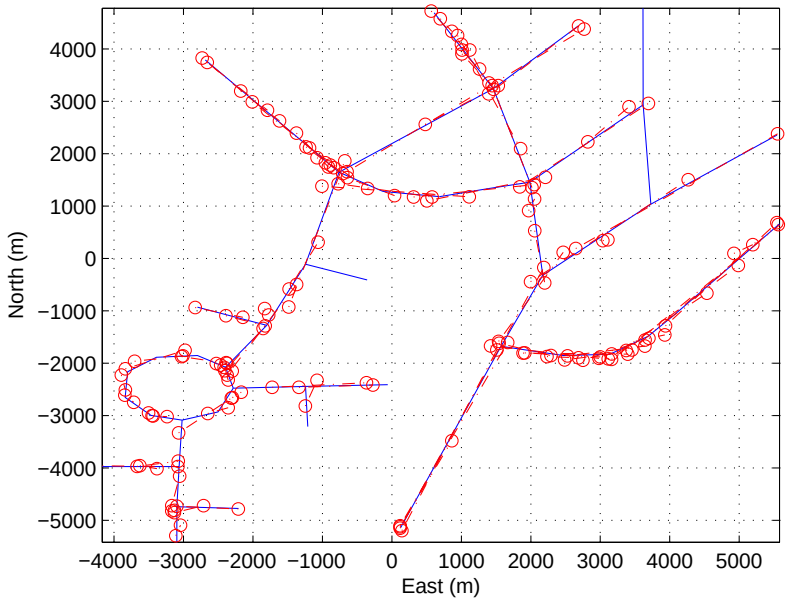

Figure 12: Estimated roads using the first 100 radar tracks with road consistence tests. Blue solid lines: true roads; red dash-dot lines+circles: estimated roads.

4.5 Road Merging

As we can see in Fig. 12, the road estimates are fragmented, with many small road segments, some of which really belong to single roads. To combine the fragmented road estimates that belong to the same road, Matlab codes have been developed for a road merging algorithm. The algorithm works as follows.

The input of the algorithm is the road estimates based on the radar data, and the output is the merged road estimates. Two sets of road estimates are maintained. The first set contains the merged road estimates, which is empty initially. The second set includes the unprocessed road estimates. At each iteration, one unprocessed road estimate from the second set is compared with the road estimates in the first set. If it can be associated with a merged road estimate from the first set, using a threshold t_{21} as discussed in Section 3.2.5, then the unprocessed road estimate will be fused with the corresponding merged road estimate, as described in Section 3.2.6, and it will be deleted from the second set. If it can not be associated with any road in the first set, then road to road association tests will be performed to see if it can be associated with any road in the second set using another threshold t_{22} . If the unprocessed road is associated to another unprocessed roads, these two roads will be fused, the fused road will be added to the first set, and both of the original roads will be deleted from the second set. If the unprocessed road can not be associated with any road in both sets, then it will be added in the first set as a new merged road and deleted from the second set as an unprocessed road.

Based on the first 1000 radar tracks, 258 road estimates have been generated and plotted in Fig. 13. The road merging algorithm has been applied to the 258 road estimates, and the output, the merged roads, really depends on the thresholds t_{21} and t_{22} used in the algorithm.

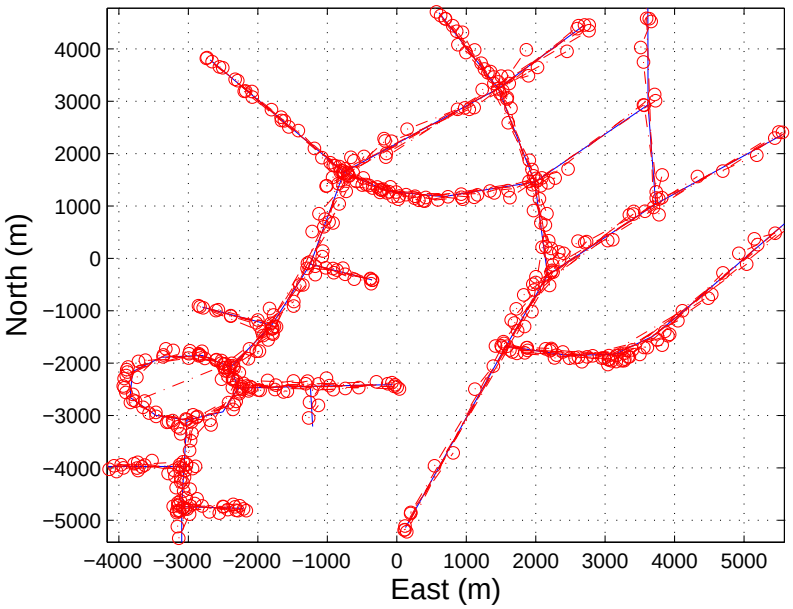

Figure 13: Estimated roads using the first 1000 radar tracks with road consistence tests. Blue solid lines: true roads; red dash-dot lines+circles: estimated roads.

In Table 1, the number of merged road estimates is listed as a function of the thresholds. Based on the numerical results, it is clear that the threshold t_{21} and t_{22} play a crucial role in road merging performance. A larger threshold means that it is easier to associate a road to another road, and hence it results in a smaller number of merged road estimates.

Table 1: Number of merged roads (N_m) based on 258 unprocessed road estimates

$t_{21} = t_{22}$	13.82	23.03	32.24	41.45	50.66	59.87	69.14
N_m	206	173	142	132	121	116	110

When $t_{21} = t_{22} = 69.14$ are used, a total of 110 merged roads have been obtained and plotted in Fig. 14. Compared to Fig. 13, in this figure, there is less number of road estimates due to the road merging procedure.

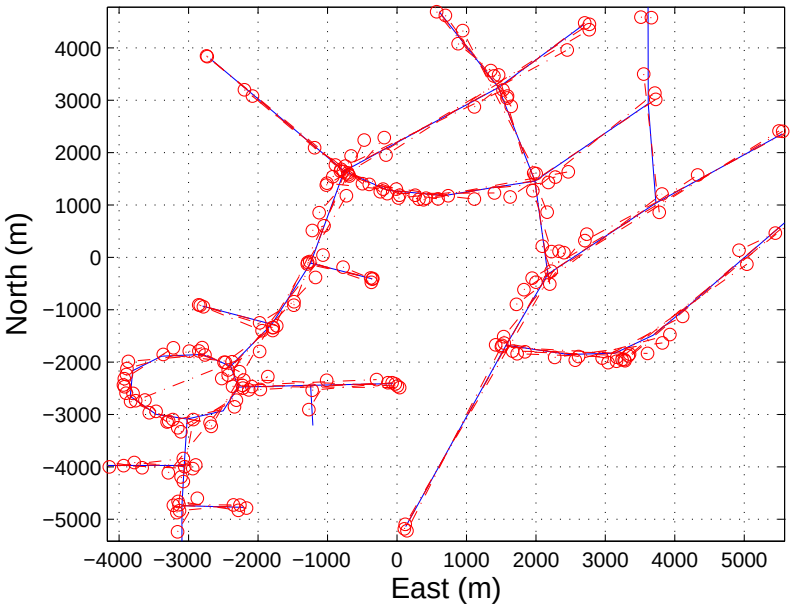

Figure 14: Merged road estimates. Blue solid lines: true roads; red dash-dot lines+circles: estimated roads.

4.6 Evaluation of Road Estimation Accuracy

In this subsection, we evaluate the road estimation accuracy of the proposed algorithm with different amount of radar track data. In this example, the 22nd road as shown in Figure 15 is chosen to illustrate the estimation accuracy. We define the absolute estimation error in road parameters a and b as $|a-\hat{a}|$ and $|b-\hat{b}|$, respectively, and compare them with the theoretical

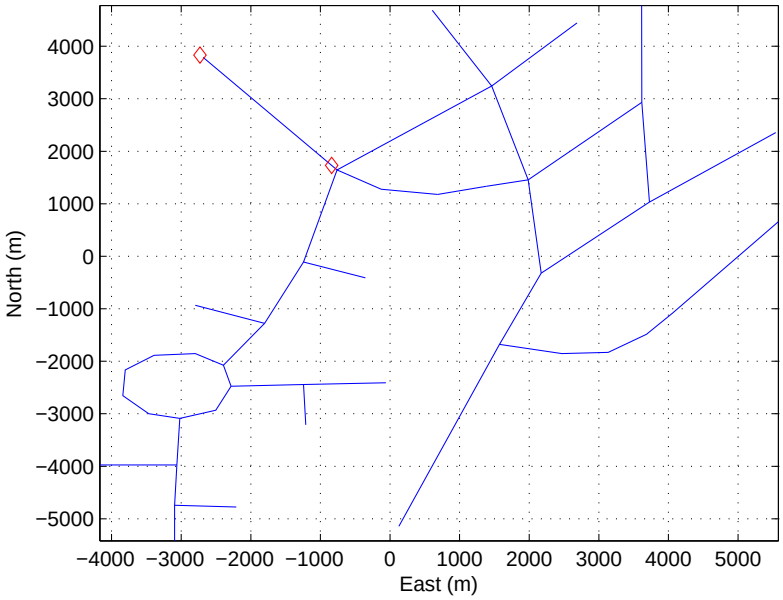

Figure 15: The 22nd road, denoted by diamonds.

CRLB on the standard deviations (s.d.s) of the estimation errors for a and b. The results based on different number of radar tracks are provided in Table 2. From this table, it is clear that as more radar track data are fused to estimate the road, the road estimation error decreases, and estimation accuracy improves significantly. Further, the calculated CRLB is comparable to the actual estimation error, and it indeed provides a very useful estimation performance measure.

Table 2: Road estimation errors

Number of radar tracks	10	20	50	100
$\lvert a - \hat{a}\rvert$	0.028	0.0011	0.0034	0.0026
CRLB on s.d. in $\hat{a}$	0.01	0.0041	0.003	0.003
$\lvert b - \hat{b}\rvert$	48.91	6.86	3.14	3.04
CRLB on s.d. in $\hat{b}$	18.7	7.06	5.87	5.86

5 CONCLUSION

In this project, we proposed a framework to generate accurate road network map based on radar tracks of ground targets. An ML road estimator has been developed to estimate roads using radar tracks, and the corresponding CRLB matrix was derived as well. Track to

road correlation/association approaches have been proposed to associate track segments to existing road segments. To enhance the association performance, statistics and information extracted from the track estimate, including both position and velocity estimates, have been used. For tracks overlapping with any existing roads, a track to road fusion algorithm was proposed to fuse the track with the associated road segments to improve the road map accuracy. Some numerical examples have been provided to demonstrate the effectiveness of the proposed approaches.

References

[1] T. Kirubarajan, Y. Bar-Shalom, K.R. Pattipati, and I. Kadar, "Ground Target Tracking with Variable Structure IMM Estimator," *IEEE Trans. on Aerospace and Electronic Systems*, vol. 36, no. 1, pp. 26–46, 2000.

[2] M. Ulmke and W. Koch, "Road-Map Assisted Ground Moving Target Tracking," *IEEE Trans. on Aerospace and Electronic Systems*, vol. 42, no. 4, pp. 1264–1274, 2006.

[3] J.S. Bergin, P.M. Techau, W.L. Melvin, and J.R. Guerci, "GMTI STAP in Target-Rich Environments: Site-Specific Analysis," in *Proc. of 2002 IEEE National Radar Conference*, Long Beach, CA, April 2002, pp. 391–396.

[4] C.T. Capraro, G.T. Capraro, I. Bradaric, D.D. Weiner, M.C. Wicks, and W.J. Baldygo, "Implementing Digital Terrain Data in Knowledge-Aided Space-Time Adaptive Processing," *IEEE Trans. on Aerospace and Electronic Systems*, vol. 42, no. 3, pp. 1080–1099, 2006.

[5] S. D. O'Neil, "Estimating Road Networks Using Archived GMTI Data," in *Proc. of the IEEE Aerospace Conference*, Big Sky, MT, March 2001, vol. 4, pp. 1865–1871.

[6] W. Koch, J. Koller, and M. Ulmke, "Ground target tracking and road map extraction," *ISPRS Journal of Photogrammetry and Remote Sensing*, vol. 61, no. 3-4, pp. 197–208, December 2006.

[7] S.E. Sklarz, A. Novoselsky, and M. Dorfan, "Incremental Fusion of GMTI Tracks for Road Map Estimation," in *Proc. of the 11th International Conference on Information Fusion*, Cologne, Germany, June 2008.

[8] W. Song, J. M. Keller, T. L. Haithcoat, and C. H. Davis, "Automated geospatial conflation of vector road maps to high resolution imagery," *IEEE Trans. Image Processing*, vol. 18, no. 2, pp. 388–400, February 2009.

[9] S. Movaghati, A. Moghaddamjoo, and A. Tavakoli, "Road extraction from satellite images using particle filtering and extended kalman filtering," *IEEE Trans. Geoscience and Remote Sensing*, vol. 48, no. 7, pp. 2807–2817, July 2010.

[10] Y. Bar-Shalom, P.K. Willett, and X. Tian, *Tracking and Data Fusion: A Handbook of Algorithms*, YBS Publishing, Storrs, CT, 2011.

[11] L.M. Kaplan, Y. Bar-Shalom, and W.D. Blair, "Assignment costs for multiple sensor track-to-track association," *IEEE Transactions on Aerospace and Electronic Systems*, vol. 44, no. 2, pp. 655–677, April 2008.

[12] "Coordinate Conversions and Transformations including Formulas," July 2011, OGP Publication 373-7-2, Geomatics Guidance Note Number 7, part 2.

[13] R.A. Horn and C. R. Johnson, *Matrix Analysis*, Cambridge University Press, New York, NY, 1985.

List of Acronyms

CRLB Cramer-Rao Lower Bound

DTW Dynamical Time Warping

GMTI Ground Moving Target Indicator

ML Maximum Likelihood

MLE Maximum Likelihood Estimator

NIMA National Imagery and Mapping Agency

SAR Synthetic Aperture Radar

STAP Space-Time Adaptive Processing

USGS United States Geological Survey